N<inf>2</inf>O Formation during NH<inf>3</inf>-SCR over Different Zeolite Frameworks: Effect of Framework Structure, Copper Species, and

Downloaded from: https://research.chalmers.se, 2025-06-18 04:23 UTC

Citation for the original published paper (version of record):
Han, J., Wang, A., Isapour Toutizad, G. et al (2021). N<inf>2</inf>O Formation during NH<inf>3</inf>-SCR over Different Zeolite Frameworks: Effect of Framework Structure, Copper Species, and Water. Industrial & Engineering Chemistry Research, 60(49): 17826-17839. http://dx.doi.org/10.1021/acs.iecr.1c02732

N.B. When citing this work, cite the original published paper.

research.chalmers.se offers the possibility of retrieving research publications produced at Chalmers University of Technology. It covers all kind of research output: articles, dissertations, conference papers, reports etc. since 2004. research.chalmers.se is administrated and maintained by Chalmers Library

(article starts on next page)

I&EC research
Industrial & Engineering Chemistry Research
pubs.acs.org/IECR
Article

N_2O Formation during NH_3-SCR over Different Zeolite Frameworks: Effect of Framework Structure, Copper Species, and Water

Joonsoo Han, Aiyong Wang, Ghodsieh Isapour, Hanna Härelind, Magnus Skoglundh, Derek Creaser, and Louise Olsson*

Cite This: *Ind. Eng. Chem. Res.* 2021, 60, 17826−17839

Read Online

ACCESS | Metrics & More | Article Recommendations | Supporting Information

ABSTRACT: The formation characteristics of N_2O were investigated with respect to copper-functionalized zeolites, i.e., Cu/SSZ-13 (CHA), Cu/ZSM-5 (MFI), and Cu/BEA (BEA) and compared with the corresponding zeolites in the H form as references to elucidate the effect of the framework structure, copper addition, and water. Temperature-programmed reduction with hydrogen showed that the CHA framework has a higher concentration of Cu^{2+} (Z2Cu) compared to MFI and BEA. The characterizations and catalyst activity results highlight that CHA has a framework structure that favors high formation of ammonium nitrate (AN) in comparison with MFI and BEA. Moreover, AN formation and decomposition were found to be promoted in the presence of Cu species. On the contrary, lower N_2O formation was observed from Cu/CHA during standard and fast SCR reactions, which is proposed to be due to highly stabilized AN inside the zeolite cages. On the other hand, significant amounts of N_2O were released during heating due to decomposition of AN, implying pros and cons of AN stability for Cu/CHA with possible uncontrolled N_2O formation during transient conditions. Additionally, important effects of water were found, where water hinders AN formation and increases the selectivity for decomposition to NO_2 instead of N_2O. Thus, less available AN forming N_2O was observed in the presence of water. This was also observed in fast SCR conditions where all Cu/zeolites exhibited lower continuous N_2O formation in the presence of water.

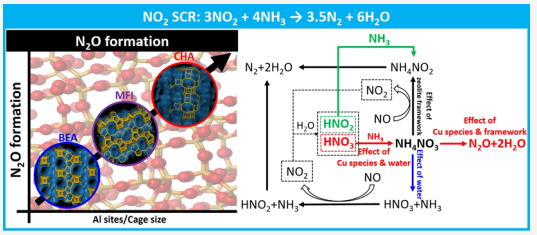

INTRODUCTION

Nitrous oxide (N_2O) is a strong greenhouse gas (GHG), which is 297 times more potent than CO_2.[1] It is therefore critical to minimize N_2O formation in after-treatment systems during reduction of nitrogen oxides (NOx). Achieving higher NOx conversion results in increased N_2O emissions over conventional after-treatment systems such as selective catalytic reduction (SCR) and SCR combined with an ammonia slip catalyst (ASC).[2] Furthermore, N_2O may also be formed over the diesel oxidation catalyst (DOC) commonly used in the after-treatment system.[3] Therefore, significant system optimization has to be considered to satisfy future demanding emission legislation for N_2O.[4]

Selective catalytic reduction of NOx by NH_3 (NH_3−SCR) is well known as one of the leading NOx abatement technologies, especially urea-SCR in the automotive industry. Urea-SCR systems selectively convert engine-out NOx emissions to nitrogen (N_2) and water by using NH_3 resulting from thermal decomposition and hydrolysis of a urea solution. However, N_2O is produced as one of the by-products during the SCR reactions of NOx over a wide temperature range.[2,5−8] Thermal decomposition of ammonium nitrate (AN) has been reported to be the main source of N_2O formation at low temperature.[7−10] In the high-temperature region, both unselective ammonia oxidation and SCR reactions can result in N_2O formation.[7,8,11] The development of robust novel catalyst materials having excellent DeNOx performance and lower N_2O formation is therefore necessary.

In NH_3-SCR chemistry, for NOx reduction over Cu/zeolites, three major reaction pathways are generally described according to the amount of NO_2 in the feed. In the standard SCR reaction, equimolar amounts of NO and NH_3 react in the presence of O_2 ($4NO + 4NH_3 + O_2 \rightarrow 4\ N_2 + 6H_2O$). This is a redox reaction as evident from operando experiments, where both Cu^+ and Cu^{2+} were observed.[12−16] In the presence of equimolar amounts of NO and NO_2, the SCR reaction rate is considerably promoted through the fast SCR reaction ($2\ NO + 2\ NO_2 + 4NH_3 \rightarrow 4\ N_2 + 6H_2O$).[17−19] On the contrary, when the amount of NO_2 is higher than the amount of NO, the SCR reaction rate is slower compared to the fast SCR reaction, and the reaction is denoted as the slow SCR reaction ($6NO_2 + 8NH_3 \rightarrow 7\ N_2 + 12H_2O$).[18−20] It has been reported that the N_2O formation in the low-temperature region increases when the NO_2 fraction in the feed is increased due to the formation and thermal decomposition of ammonium nitrate

Received: July 18, 2021
Revised: November 21, 2021
Accepted: November 21, 2021
Published: November 30, 2021

Downloaded via CHALMERS UNIV OF TECHNOLOGY on December 20, 2021 at 14:33:47 (UTC).
See https://pubs.acs.org/sharingguidelines for options on how to legitimately share published articles.

ACS Publications
© 2021 The Authors. Published by American Chemical Society

https://doi.org/10.1021/acs.iecr.1c02732
Ind. Eng. Chem. Res. 2021, 60, 17826−17839

(AN).[7,9,10,21,22] The formation and accumulation of AN can cause fouling or masking of the zeolite channels as well as inhibition of the SCR reactions, resulting in temporary deactivation.[9,10,19] In addition, higher N_2O formation is typically observed from the zeolites having larger pore dimensions (e.g., BEA framework) in comparison with zeolites having medium or smaller pore dimensions (e.g., MFI and CHA framework).[21,23,24]

Copper-exchanged chabazite (Cu/CHA) has received considerable attention and been successfully commercialized for the use in exhaust after-treatment systems thanks to high activity at low temperature with high selectivity for N_2 formation and excellent thermal stability with low N_2O formation.[8,21,23] Cu/SSZ-13, with the CHA framework, exhibits significantly lower N_2O formation in comparison with ZSM-5 and BEA zeolites having medium and large pore sizes, respectively. Up to now, several research groups have reported that the N_2O formation from Cu-supported zeolites follows the order of small pore < medium pore < large pore, due to the thermal stability of AN inside the catalyst pores.[21,23−25] As mentioned above, thermal decomposition of AN has been reported as the main source of N_2O formation for Cu-functionalized zeolites in the low-temperature region. Dedicated research work has been done by conducting transient experiments with AN to understand the N_2O formation mechanism at low temperature. Mihai et al.[26] observed three N_2O desorption regions based on transient experiments with AN on Cu/BEA with varying Cu loadings, where more N_2O was observed when increasing the Cu loading. Recently, Feng et al.[27] proposed that low-temperature formation of N_2O in Cu/CHA is connected with H_2NNO decomposition over Cu−OOH−Cu complexes, which can explain why the N_2O formation increases with increasing copper loading at low temperatures. Furthermore, Chen et al.[21] proposed that the main reason for lower N_2O formation in Cu/CHA is owing to the lower activity for NO oxidation and subsequent surface nitrate formation, although higher stability of AN resulted from the pore-confinement effect of the CHA structure in comparison with Cu/BEA. Recently, Kubota et al.[22] proposed that Brønsted acid sites catalyze the decomposition of NH_4NO_3 into N_2O and H_2O based on AN temperature-programmed desorption experiments supplemented by density functional theory calculations for H/AFX zeolites. Further, they suggested that the formation of the H_2NNO_2 intermediate is the rate-determining step with an energy barrier of 138 kJ mol^{-1}. The reasons for the increased SCR activity and concurrent reduction in N_2O formation in small-pore copper zeolites is still under discussion. However, there are to our knowledge no studies available in the literature that examines if it is the zeolite framework or different Cu species that are responsible for different N_2O formations for different Cu/zeolites in the presence of NH_3 and NO_2. In addition, the effect of water on the N_2O formation over Cu/CHA is not well established to our knowledge.

The objective of this study is therefore to examine the N_2O formation over zeolites with different framework structures, more specifically BEA (BEA), ZSM-5 (MFI), and SSZ-13 (CHA), both in the H form and exchanged with copper. Furthermore, the effect of water addition on the mechanism for N_2O formation is studied. The N_2O formation is examined by ammonium nitrate temperature-programmed desorption experiments as well as flow reactor experiments with standard and fast SCR conditions. Zeolite samples in the H form were used as references to observe the effect of Cu species on AN formation and decomposition. The flow reactor experiments were combined with detailed characterization by elemental analysis, nitrogen sorption, X-ray diffraction, in situ infrared spectroscopy, and hydrogen temperature-programmed reduction to gain increased understanding about N_2O formation over these catalysts.

EXPERIMENTAL SECTION

Sample Preparation. The Na/SSZ-13 (CHA, small-pore size) zeolite was synthesized based on the method described by Gao et al.[28] Details regarding the synthesis procedure of Na/SSZ-13 and the conversion to NH_4/SSZ-13 can be found in the Supporting Information (SI).

The prepared NH_4/SSZ-13 was transformed into copper form using a conventional incipient wetness impregnation (IWI) method to introduce copper species into the zeolites (e.g., SSZ-13). A total of 0.160 g of Cu $(NO_3)_2{\cdot}2.5\ H_2O$ (98%, Sigma-Aldrich, pentahydrate, 223395-500G) was completely dissolved into 3 g of ethanol. Thereafter, 2 g of prepared NH_4/SSZ-13 zeolite was carefully introduced into the mixture, and then the mixture was capped for 15 min, while continuing the stirring. Subsequently, the resulting mixture was dried at room temperature overnight, after which it was well-crushed to a fine powder. Finally, the resulting powder was calcined at 600 °C for 8 h and 750 °C for 2 h, with a heating rate of 2 °C·min^{-1}.

The ammonium forms of ZSM-5 (CBV2314, ZEOLYST International) and BEA (CP814E, ZEOLYST International) zeolite powder samples were directly used. The copper forms of ZSM-5 and BEA were prepared from the NH_4/ZSM-5 and NH_4/BEA zeolite samples by following the same IWI procedure as for Cu/SSZ-13, described above. Note that during the IWI, the amount of ethanol was slightly modified for the BEA zeolite due to its lower density compared to SSZ-13 and ZSM-5. Namely, 6 g of ethanol was used for BEA zeolite.

The H forms of SSZ-13, ZSM-5, and BEA were prepared using the prepared NH_4/SSZ-13, NH_4/ZSM-5, and NH_4/BEA samples. These ammonium form zeolites were calcined by following the same calcination conditions as for the preparation of Cu/SSZ-13. In summary, six different catalysts were prepared in total, i.e., both copper and hydrogen forms of SSZ-13, ZSM-5, and BEA.

The six different zeolite powder samples were washcoated onto honeycomb-structured cordierite monoliths (400 cpsi, 15 mm × 20 mm). The prepared catalyst powder sample was added to a solution (50 wt % ethanol +50 wt % Milli-Q water) together with Boehmite as binder (Disperal P2, Sasol). The washcoat was composed of 95 wt % of the prepared zeolite and 5 wt % of the binder. A pre-calcined (at 600 °C for 2 h) monolith was dipped into the mixture. After each dipping, the monolith was mildly dried using a hot air gun at around 80 °C to avoid channel clogging, with a subsequent drying step at 500 °C for 1 min. The loading procedure was repeated until the desired loading (300 mg) of washcoat was reached. The six dried monolith catalysts were then calcined at 500 °C for 2 h, with a heating ramp of 2 °C·min^{-1}.

Sample Characterization. *Sample Composition and Structure.* Elemental analysis of the prepared catalyst powder samples was carried out using inductively coupled plasma sector field mass spectrometry (ICP-SFMS) at ALS Scandinavia AB.

https://doi.org/10.1021/acs.iecr.1c02732
Ind. Eng. Chem. Res. 2021, 60, 17826−17839

Powder X-ray diffraction (XRD) was performed with fresh powder samples to verify the crystalline structure by a SIEMENS diffractometer D5000 operating at 40 kV, using the Kα_1 radiation of a Cu anode as the X-ray source (λ = 1.54060 Å).

The specific surface area of the samples was measured by nitrogen sorption using the Brunauer−Emmett−Teller (BET) method. Before the measurement, the powder samples were degassed at 250 °C for 6 h under N_2 feeding. A Micromeritics Tri-Star 3000 instrument was used to measure the N_2 adsorption and desorption isotherms at 77 K. Additionally, the pore volume was calculated based on the t-plot method. Note that fresh zeolite samples in the H form and degreened Cu/zeolite samples were used for the measurement.

In situ diffuse reflectance infrared Fourier transform spectroscopy (DRIFTS) was carried out on the prepared Cu/zeolite powder samples (i.e., Cu/SSZ-13, Cu/ZSM-5, and Cu/BEA) to characterize the copper species by observing the antisymmetric T−O−T vibrational region perturbed by Cu cations in the presence of NH_3. The samples (about 50−60 mg) were placed in a heated reaction cell covered with CaF_2 windows (Harrick Scientific, Praying Mantis) and mounted on a Vertex 70 FT-IR spectrometer (Bruker) equipped with a liquid N_2-cooled mercury cadmium telluride (MCT) detector. The temperature was controlled by a PID regulator (Eurotherm 2416), and mass flow controllers (Bronkhorst Hi-Tech) were used to supply the reactant gases into the reaction cell. The reported temperatures in the DRIFTS experiments were measured by a thermocouple located in the sample bed inside the reaction cell. Before the DRIFTS experiment, the calcined powder samples were degreened in a crucible inside a horizontal quartz tube in a flow reactor under standard SCR conditions as described in the Catalytic Activity Measurements section. The color of the degreened Cu/zeolite samples turned from light green into pastel blue after degreening, indicating copper migration into ion-exchange sites.[29] Thereafter, the degreened powder sample was placed in the DRIFTS reaction cell. Prior to the tests, the powder sample was pretreated in flowing 10% O_2, Ar bal at 288 °C for 1 h and then cooled to the desired temperature (ca. 150 °C). Thereafter, 300 ppm NH_3 + 10% O_2 + Ar were steadily fed for 1 h. DRIFTS spectra were recorded (accumulation of 256 scans, resolution of 4 cm^{-1}) versus time under a gas flow rate of 100 mL·min^{-1}. The outlet gases leaving the reaction cell were monitored by mass spectrometry (Hiden HPR-20 QUI MS).

Hydrogen Temperature-Programmed Reduction. Hydrogen temperature-programmed reduction (H_2-TPR) was performed for the Cu/zeolite samples to elucidate the reduction characteristics of the copper species by differential scanning calorimetry (DSC) using a Sensys DSC calorimeter from Setaram. The outlet gases from the calorimeter were detected by mass spectrometry (Hiden HPR-20 QUI MS). First, the powder sample was degreened in the flow reactor, see the Catalytic Activity Measurements section. It should be noted that the catalyst was exposed to air between the flow reactor experiment and the H_2 TPR experiment and then no pre-treatment was performed in the calorimeter in order to have the samples in the hydrated form. A total of 60 mg of sample (corresponding to roughly 20 μmol of Cu based on ICP test) was placed in the calorimeter and exposed to 0.2% H_2/Ar for 20 min at room temperature in 20 mL·min^{-1} of total flow rate. This was followed by increasing the temperature to 800 °C with a rate of 10 °C·min^{-1}, while exposing the sample to the same gas mixture. Finally, the temperature was kept constant at 800 °C for 30 min using 0.2% H_2/Ar. The experiment was conducted with hydrated samples, i.e., no pre-treatment was conducted prior to the H_2-TPR experiment.

Ammonia Temperature-Programmed Desorption. Ammonia temperature-programmed desorption (NH_3−TPD) was conducted in the flow reactor (see the Catalytic Activity Measurements section) and was used to measure the adsorbed NH_3 on Lewis and Brønsted acid sites in the prepared monolith samples. After the degreening treatment (see the Catalytic Activity Measurements section), the TPD was conducted as follows: (i) heating the monolith to 500 °C in 10% O_2 and 5% H_2O and then keeping the temperature constant at 500 °C for 20 min, (ii) decreasing the temperature to 100 °C in the same gas mixture, (iii) introducing 400 ppm NH_3 and 5% H_2O for 1 h, (iv) switching off the NH_3 flow and purging with 5% H_2O in Ar for 30 min to remove weakly adsorbed NH_3 on the sample at the adsorption temperature, and (v) keeping the purging gas mixture (5% H_2O in Ar) when increasing the temperature to 500 °C using a heating rate of 20 °C·min^{-1} and finally keeping the temperature constant at 500 °C for 20 min while exposing the catalyst to 5% H_2O in Ar. The total flow was 1.2 L·min^{-1} corresponding to a gas hourly space velocity (GHSV) of 20,400 h^{-1}.

Ammonium Nitrate Temperature-Programmed Desorption. Ammonium nitrate temperature-programmed formation and desorption (AN-TPD) was performed using monolith samples in the flow reactor (see the Catalytic Activity Measurements section), both above and below the AN decomposition temperature (170 °C[30]). The inlet gas lines were carefully heated to 191 °C to avoid AN formation and condensation of water vapor during the measurements. The outlet gases from the flow reactor were analyzed by mass spectrometry (Hiden HPR-20 QUI MS) to measure nitrogen formation, and the other gases were measured using FT-IR (see the Catalytic Activity Measurements section). Several pre-tests were conducted without sample to confirm that no AN was formed in the reactor system during the tests. The results for one of these pre-tests are shown in Figure S1 (Supporting Information). After degreening and pretreatment (see the Catalytic Activity Measurements section), the AN-TPD experiment was conducted. The reactants (i.e., 200 ppm NH_3, 200 ppm NO_2, 10% O_2, 5% H_2O) were simultaneously introduced for 1 h during the adsorption period, and thereafter, the catalyst was flushed with 5% H_2O in Ar for 30 min. This was followed by increasing the temperature to 500 °C using a heating rate of 20 °C·min^{-1} and maintaining the same gas mixture (5% H_2O in Ar) in 1.2 L·min^{-1} of total flow rate corresponding to a GHSV of 20,400 h^{-1}. The detailed procedure of the test is specified in Figure S2. Additionally, the AN-TPD experiment was performed in the absence of water vapor for Cu/SSZ-13 to study the effect of water vapor on AN formation and decomposition. The amount of formed AN during the adsorption step was estimated by establishing nitrogen mass balance equations. Further details and the associated reactions are described in Table S1 in the Supporting Information (SI).

Catalytic Activity Measurements. The catalytic activity measurements were conducted in a laboratory scale flow reactor. The monolith sample was placed in a horizontal quartz tube (inner diameter: 16 mm). A coil around the quartz tube was used for heating, and the temperature was controlled by a Eurotherm controller. Two K-type thermocouples were used

https://doi.org/10.1021/acs.iecr.1c02732
Ind. Eng. Chem. Res. 2021, 60, 17826−17839

to measure the temperature inside one of the center channels and the temperature of the inlet gas 10−15 mm before the monolith inlet. The synthetic gas mixtures were introduced to the flow reactor using a set of mass flow controllers (MFCs) from Bronkhorst and water was supplied with a Bronkhorst controlled evaporator and mixing (CEM) system. All gas lines were carefully insulated and heated to 191 °C to avoid water condensation and ammonium nitrate formation. The outlet gases from the flow reactor were measured and monitored by FT-IR spectroscopy (Multigas2030, MKS), where the temperature of the outlet gas sampling line was maintained at 191 °C. Ar was used as inert balance in all experiments and the total flow was 1.2 L·min^{-1} corresponding to a GHSV of 20,400 h^{-1}.

Degreening and pre-treatment were performed prior to the catalytic activity tests. The monolith sample (and also the powder samples for DRIFTS and H_2-TPR) was degreened as follows: (i) exposing to 400 ppm NH_3, 400 ppm NO, 5% H_2O at 250 °C for 1 h; (ii) increasing the temperature to 500 °C while maintaining the same gas composition; and (iii) additionally adding O_2 to the gas mixture at 500 °C for 2 h under standard SCR reaction conditions. During degreening, standard SCR conditions were used to induce the migration of copper species into ion-exchanged sites inside the zeolite cages.[31] Between each experiment in the flow reactor, a pre-treatment was conducted in the presence of 10% O_2 and 5% H_2O at 500 °C for 20 min. The purpose of the pre-treatment was to clean the catalyst surface before the activity tests.

Activity tests were performed under both standard and fast SCR conditions. For standard SCR conditions, the following gas mixture was used: 400 ppm NO, 400 ppm NH_3, 10% O_2, 5% H_2O. The temperature was increased stepwise from 100 to 200 °C with 20 °C increments, and above this low-temperature region, the temperature was increased with 50 °C increments each to 500 °C. Each step was maintained for 30 min, which was enough to reach steady-state, except at 100 °C for standard SCR conditions for Cu/SSZ-13. For fast SCR conditions, 200 ppm NO, 200 ppm NO_2, 400 ppm NH_3, 10% O_2, and 5% H_2O were used. The temperature was stepwise increased from 150 to 500 °C with 50 °C increments, and each step was maintained for 30 min. For the lowest temperatures, steady state was not fully reached.

RESULTS AND DISCUSSION

In this work, we compare N_2O formation for three different zeolites, with and without functionalization with Cu, during the SCR process. SSZ-13 was studied because it is a commercial zeolite for SCR, while BEA and ZSM-5 were chosen due to their different structures to find an understanding about the structure−activity relation. Cu/SSZ-13 is resistant to hydrocarbons and has high thermal stability. The Cu/SSZ-13 sample deactivates slower during SO_2 exposure than the other two catalysts but reaches a lower conversion during time on stream (see Figure S15, SI). These results are in line with the recent study by Auvray et al.[32] where it was reported that Cu/BEA was significantly less affected than Cu/SSZ-13 from SO_2 or SO_3, and the reason for this was suggested to be less steric hindrance of Cu/BEA by sulfur species.

Sample Characterization. The ICP-SFMS, BET, and XRD experiments were done to characterize the prepared samples. Detailed information of the samples is found in the SI (Table S2 and Figure S4). A similar Si/Al ratio (~11) and Cu content (~2 wt %) of the samples was confirmed. XRD shows that both the H and Cu forms of BEA, ZSM-5, and SSZ-13 have the characteristic framework structure of BEA, MFI, and CHA, respectively.

Characterization of Cu Species. Several research groups have reported the existence of different types of Cu species in Cu loaded zeolites.[20,33−37] Kwak et al.[35] and Gao et al.[28] verified the existence of two species of Cu^{2+} ions. Specifically, there are two options for this, two framework Al atoms can be charge compensated by a single Cu^{2+} ion (Z2Cu) or the charge compensation can be done by a single framework Al charge balanced by an OH group, i.e., $[Cu(OH)]^+$ (ZCuOH).[29,38] These species have different susceptibility to reduction owing to the different binding strength with the zeolite framework. In this sense, temperature-programmed reduction with H_2 is a useful characterization technique to identify the existence of different Cu species and therefore used in the present study.

Figure 1 shows the H_2 consumption as a function of sample temperature and the normalized Cu species population for the three Cu/zeolite samples (i.e., Cu/BEA, Cu/ZSM-5, and Cu/SSZ-13). Three distinct H_2 consumption peaks are observed for all samples below 650 °C. The first peak centered between 217 and 225 °C is assigned to the reduction of highly dispersed CuO species on the external surface of the zeolite crystals.[9,38−40] This peak is rather small and is located at similar temperatures for all three samples. A number of research groups have reported that ZCuOH is more weakly

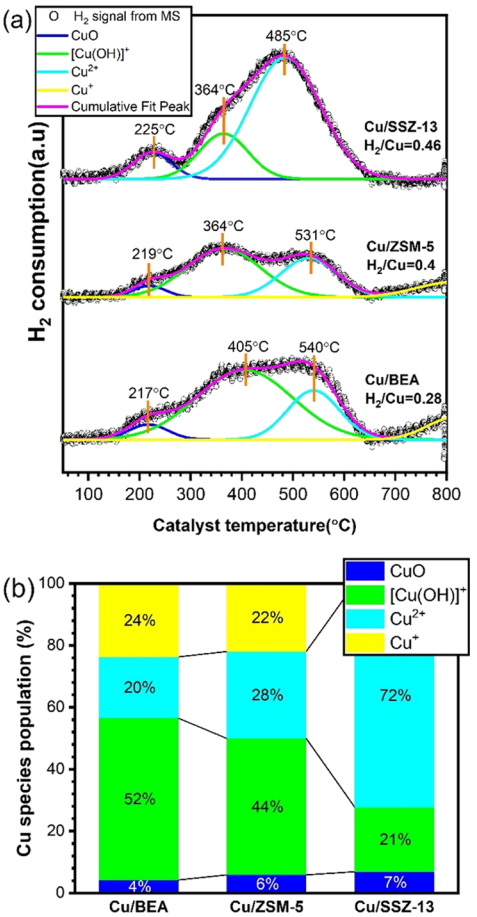

Figure 1. (a) Consumption of H_2 during H_2-TPR for the Cu/SSZ-13, Cu/ZSM-5, and Cu/BEA samples. (b) Cu species population of Cu/SSZ-13, Cu/ZSM-5, and Cu/BEA (gas inlet: 0.2% H_2/Ar, heating rate: 10 °C·min^{-1}).

https://doi.org/10.1021/acs.iecr.1c02732
Ind. Eng. Chem. Res. 2021, 60, 17826−17839

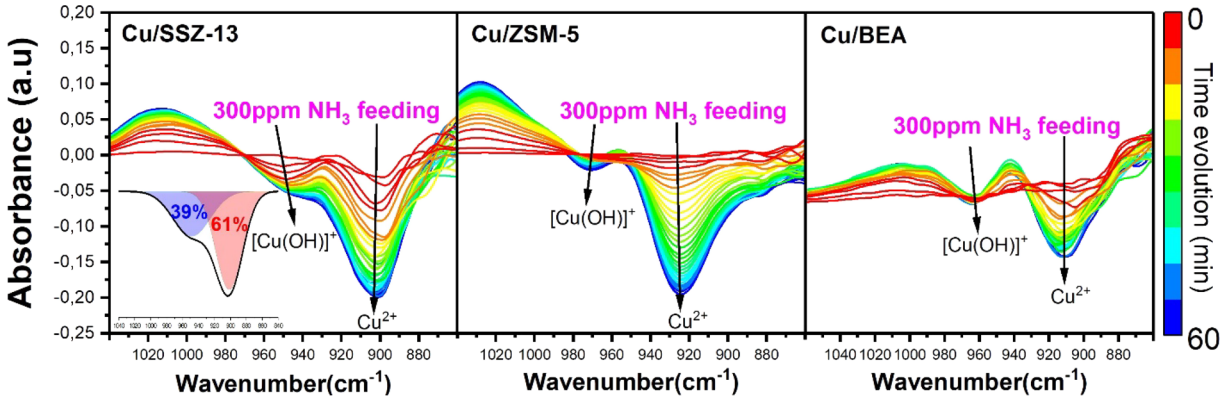

Figure 2. Comparison of DRIFTS spectra in the antisymmetric T−O−T vibrational region perturbed by Cu cations during NH_3 exposure for the Cu/SSZ-13, Cu/ZSM-5, and Cu/BEA samples. The inset illustrates the Cu cations population for Cu/SSZ-13 (gas inlet: 300 ppm NH_3, 10% O_2, Ar bal, 1 h, flow rate: 100 mL·min^{-1}, sample temperature: 150 °C).

bound to the zeolite framework than that of Z2Cu;[20,29,35,36] thus, the second (centered between 364 and 405 °C) and the third peaks (485−540 °C) are attributed to ZCuOH and Z2Cu, respectively.

According to Gao et al., Cu^+ reduction to Cu^0 was not observed for Cu/SSZ-13 since extensive Cu^+ reduction is expected only when degradation of the CHA structure occurs.[41] Wang et al. did not observe any Cu^+ reduction below 800 °C in Cu/LTA and Cu/SSZ-13.[29,38] Hence, Cu^+ reduction below 800 °C is not likely the case for Cu/SSZ-13. However, contrary to Cu/SSZ-13, complete reduction of Cu^{2+} to the metallic state (Cu^0) can occur below 800 °C for Cu/ZSM-5 and Cu/BEA.[39,42−44] The H_2 consumption profiles for both Cu/ZSM-5 and Cu/BEA suggest a two-step reduction ($Cu^{2+} \rightarrow Cu^+$ below 650 °C and $Cu^+ \rightarrow Cu^0$ above 650 °C). Furthermore, the calculated H_2/Cu ratios in the present study are below 0.5, which suggests that auto reduction also occurs during the reduction of Cu^{2+}, since Cu^+ reduction is observed above 650 °C. Hajjar et al. proposed the existence of two types of framework Al sites in zeolite BEA.[45] Ayo et al. confirmed isolated tetrahedrally and octahedrally coordinated Cu^{2+} species in Cu/BEA and Cu/ZSM-5 where no clear signs of Cu^+ reduction were observed below 650 °C.[46] Consequently, their H_2-TPR results are in line with the H_2-TPR results for Cu/ZSM-5 and Cu/BEA in the present study. It is, therefore, suggested that Cu^+ reduction occurs above 650 °C for Cu/ZSM-5 and Cu/BEA. Note that although most of the Cu^+ reduction is observed above 650 °C, any possibility of a minor contribution of complete Cu^{2+} reduction ($Cu^{2+} \rightarrow Cu^0$) cannot be ruled out below 650 °C according to the literature.[39,42−44]

In order to investigate the population of Cu cation species, the assigned H_2 consumption peaks were deconvoluted; thereafter, each corresponding peak area was normalized to the total H_2 consumption below 650 °C for each sample in Figure 1b and Table S3. The amount of the different Cu species is influenced by various factors, for example, zeolite composition (Si/Al- and Cu/Al-ratios), sample treatment and preparation history, framework topology, etc.[47] In this study, the three Cu/zeolite samples have similar Si/Al- and Cu/Al-ratios as well as identical sample preparation and experimental conditions. We can therefore discuss the distribution of Cu species in terms of the effect of the zeolite framework. Figure 1b shows the population of Cu species with respect to the different framework structures. Interestingly, a high amount of Cu^{2+} (72% Z2Cu) and only 21% of $[Cu(OH)]^+$ (ZCuOH) is present in the Cu/SSZ-13 sample (small-pore zeolite). For the Cu/ZSM-5 sample (medium-pore zeolite), the corresponding figures are 28 and 44%, and for the Cu/BEA sample (large-pore zeolite), the amounts of Cu^{2+} and $[Cu(OH)]^+$ are 20 and 52%, respectively. According to Paolucci et al.,[47] two Al in a 6-membered ring (MR) with a random Al distribution in SSZ-13 are the preferred sites for Cu^{2+} exchange. These sites are saturated before the remaining 1-Al sites are populated with ZCuOH based on experimental and computational findings,[47] which is also in line with our results. Deka et al. reported that the location of copper species for Cu/ZSM-5 are in 5- or 6-membered ring subunits facing the 10-membered ring windows of the MFI framework or 6-membered ring structures facing the 12-membered ring windows of BEA framework for Cu/BEA.[48] In this respect, it seems that Al atoms are mainly distributed close to the pore opening of the channel and in the channel intersection but differently distributed in different frameworks. As described earlier, the Z2Cu requires two Al sites and ZCuOH needs one Al site as nearest neighbors in the zeolite framework. It is thereby possible that a higher number of 2-Al sites can exist in the smaller cage framework system. Consequently, we suggest that Cu/SSZ-13 has a relatively high number of 2-Al sites in the framework followed by Cu/ZSM-5 and Cu/BEA. To conclude, the three zeolites have different framework structures but also likely different amounts of 2-Al sites, resulting in different distributions of the Cu sites, which also can be one reason for their different activity for different reactions.

For further investigation of the Cu speciation in relation to the structure of the zeolites, an in situ DRIFTS study was conducted, where the T−O−T vibration region perturbed by NH_3 was investigated. Moreover, the O−H vibration region was also studied and these results can be found in the SI (Figure S5). The presence of Cu cations leads to local framework perturbation, which is examined by analyzing the T−O−T vibration region. The frequency of the antisymmetric T−O−T vibration of the O_f (denoted framework oxygen), is sensitive to the interaction with Cu cations. Furthermore, also binding with the guest ligands (i.e., NH_3 in this study) to the Cu cations results in further modification of the cation−O_f interaction. Consequently, the presence of Cu cations results in IR band displacement from the position characteristic of the unperturbed ring (1020−1100 cm^{-1}).[49] It is, thus, possible to distinguish different cationic sites, the strength of the cation-O_f

https://doi.org/10.1021/acs.iecr.1c02732
Ind. Eng. Chem. Res. 2021, 60, 17826−17839

bonds, and the interaction with an extra framework ligand.[50] Accordingly, in situ DRIFTS was carried out to investigate the effect on the zeolite framework due to the presence of different Cu cations and their populations. The degreened samples were pretreated in 10% O_2/Ar for 1 h at 288 °C; afterward, the background was measured at 150 °C in 10% O_2/Ar.

Figure 2 displays the antisymmetric T−O−T vibration region perturbed by Cu cations interacting with NH_3 with respect to the Cu/zeolites having different framework structures. Two well-resolved negative bands are clearly observed for the Cu/SSZ-13 sample. It is, however, an overlap of the negative and positive bands of ZCuOH observed for Cu/ZSM-5 and Cu/BEA. It should be noted that the experiments were repeated and the same overlap was observed. Negative bands at approximately 901 and 948 cm^{-1} are detected for Cu/SSZ-13, which correspond to Z2Cu and ZCuOH species, respectively.[29,35,38,51] It is observed that the Z2Cu band develops relatively quickly compared to that of the ZCuOH band after the introduction of NH_3. Thereafter, the ZCuOH band becomes saturated while the Z2Cu band continuously increases for all samples. This suggests that NH_3 preferentially adsorbs onto Z2Cu sites first rather than on ZCuOH sites, indicating a stronger interaction between Z2Cu sites and NH_3 molecules. This is because the Gibbs free energy for Z2Cu is lower than for ZCuOH; thus, NH_3 molecules preferentially interact with Z2Cu rather than ZCuOH.[12]

Meanwhile, these two negative bands are shifted in the case of Cu/ZSM-5 and Cu/BEA. According to Kwak et al.[35] these IR bands are due to the perturbation of the T−O−T bond and the extent of the perturbation depends on properties such as the valance state and cation position, which influence the shift of the band. According to Broclawik et al.,[51] the stronger Cu cation−O_f interaction indicates a higher extent of ring perturbation; therefore, it results in a higher band shift ($\Delta\nu$) from the position of the unperturbed ring (1020 cm^{-1}). The corresponding band positions and band shifts for ZCuOH and Z2Cu are summarized in Table 1. Higher band shifts for Z2Cu are observed in comparison with ZCuOH for all Cu/zeolite samples, indicating stronger Z2Cu interactions with the O_f than that of ZCuOH. For the interaction of ZCuOH and Z2Cu with respect to the different frameworks, the extent of the band shift for Cu/SSZ-13 is 72 and 119 cm^{-1}, respectively, and then followed by Cu/BEA and Cu/ZSM-5 (see Table 1), suggesting that the strength of the interactions increases in the following sequence: Cu/ZSM-5 < Cu/BEA < Cu/SSZ-13. Giordanino et al. have reported the same order through UV−vis−NIR spectroscopy by observing the d−d transition of Cu^{2+} with respect to Cu/BEA, Cu/ZSM-5, and Cu/SSZ-13.[52] The authors explain that this indicates that Cu^{2+} complexes are more distorted for Cu/SSZ-13 in comparison with Cu/ZSM-5 and Cu/BEA. Also, Deka et al. have confirmed the higher conformational change of the Cu^{2+} local environment for Cu/SSZ-13 by measuring the average Cu−O distance through synchrotron-based in situ XAFS/XRD measurements.[53]

Table 1. Position of Skeletal Band in Cu Cations in the Different Zeolite Framework and Displacement of T−O−T Skeletal Band ($\Delta\nu$/cm^{-1}) upon the Adsorption of NH_3 from DRIFTS for the Cu/SSZ-13, Cu/ZSM-5, and Cu/BEA Powder Samples

	position of skeletal band		band shift[a]	
sample	ZCuOH (ν/cm^{-1})	Z2Cu (ν/cm^{-1})	ZCuOH ($\Delta\nu$/cm^{-1})	Z2Cu ($\Delta\nu$/cm^{-1})
Cu/BEA	962	914	58	106
Cu/ZSM-5	970	924	50	96
Cu/SSZ-13	948	901	72	119

[a]The band shift indicates the displacement of the position of the skeletal band from the unperturbed ring (1020 cm^{-1}).

For further confirmation of the H_2-TPR results, peak deconvolution was conducted for Cu/SSZ-13 but not for the Cu/ZSM-5 and Cu/BEA samples due to overlapping between negative and positive bands during the measurement (see the inset for Cu/SSZ-13 in Figure 2). Although the integrated intensity of the ZCuOH and Z2Cu bands do not provide the exact amount of these Cu cations, a semiquantitative evaluation of the amount of Cu cations is possible.[49] It shows a 39% fraction of ZCuOH and 61% of Z2Cu. This result well supports the Cu cation population estimated by the H_2-TPR experiment for Cu/SSZ-13; therefore, it is believed that Cu/SSZ-13 has a higher quantity of 2-Al framework sites.

Ammonia and Ammonium Nitrate Interactions with the H and Cu Forms of Zeolites with Different Frameworks. NH_3-TPD was carried out using monolith samples to determine the concentration and acid strengths in each of the prepared H and Cu forms of the zeolite samples (see Figure 3). First, two distinct peaks are observed for the H/zeolites samples. The first peak is assigned to weakly adsorbed NH_3 and the second peak to Brønsted acid sites based on the DRIFTS results in Figure S5. Especially, strong Brønsted acid sites are observed for H/SSZ-13 (peak temperature 390 °C) followed by H/ZSM-5 (peak temperature 310 °C) and H/BEA (peak temperature 270 °C).

Additional peak development is clearly observed at intermediate temperatures for the Cu/SSZ-13 sample, since the strength of the Brønsted acid sites is stronger than that of the Lewis acid sites. Although a clear intermediate peak development is not observed for the Cu/ZSM-5 or Cu/BEA samples, our DRIFTS results demonstrate a clear interaction between ammonia and Lewis acid sites, i.e., Cu species (Figure S5). Moreover, the NH_3-TPD results clearly show storage of ammonia also for the Cu/BEA and Cu/ZSM-5 samples, especially for Cu/ZSM-5 where the amount of ammonia desorbed is significantly higher compared to H/ZSM-5. The reason for the absence of a clearly observably peak for ammonia desorption from Lewis acid sites is the excessive overlap with ammonia desorption from Brønsted acid sites.

Further, the NH_3 storage was investigated by integrating the TPD profiles and the results are depicted in a bar graph next to the TPD profiles in Figure 3. Among the samples in the H form, H/SSZ-13 shows the highest amount NH_3 stored and it is similar for H/BEA. However, H/ZSM-5 exhibits significantly lower ammonia storage capacity. The Cu/zeolite samples show higher NH_3 storage capacity compared to the corresponding samples in the H form. This is reasonable since Lewis acid sites can adsorb NH_3, where Z2Cu (binding to 2-Al sites) can interact with up to four NH_3 molecules and ZCuOH (binding to 1-Al sites) can interact with three NH_3 molecules. On the other hand, only one NH_3 molecule can adsorb on the Brønsted acid sites, i.e., Si−O(H)−Al; thus, it is reasonable to expect an increased NH_3 storage for Cu/zeolites. The Cu/SSZ-13 and Cu/ZSM-5 samples show higher NH_3 storage capacity in comparison with Cu/BEA but different contribu-

https://doi.org/10.1021/acs.iecr.1c02732
Ind. Eng. Chem. Res. 2021, 60, 17826−17839

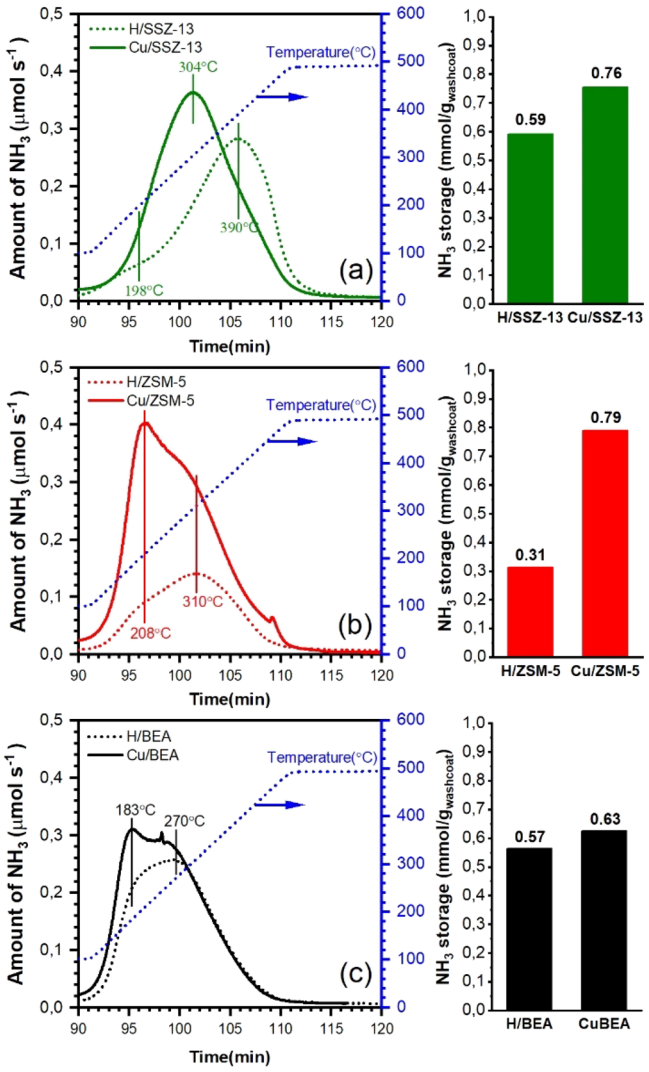

Figure 3. Ammonia temperature-programmed desorption with respect to the prepared samples in the H and Cu forms of CHA (a), ZSM-5 (b), and BEA (c). The bar graphs to the right of the NH_3 profiles indicate normalized ammonia storage (gas inlet during adsorption: 400 ppm NH_3, 5% H_2O in Ar for 1 h at 100 °C, flow rate: 1200 mL·min^{-1}, heating rate: 20 °C·min^{-1}).

tions of the adsorption sites are observed. A significant contribution from Lewis acid sites is observed for the Cu/SSZ-13 sample compared to Cu/ZSM-5 and Cu/BEA, whereas for Cu/ZSM-5, an important contribution comes from both weakly adsorbed NH_3 and NH_3 on Lewis acid sites. Remarkably, a larger difference in NH_3 storage between H/ZSM-5 and Cu/ZSM-5 is observed after impregnation of Cu^{2+} ions in the case of ZSM-5, and the possible reason can be related to the relatively lower surface area for H/ZSM-5 (see Table S2) compared to H/SSZ-13 and H/BEA. Moreover, a substantial amount of Lewis acid sites at intermediate temperatures (peak temperature 304 °C) is observed with a decreased amount of ammonia on Brønsted acid sites (peak temperature 390 °C) for Cu/SSZ-13, indicating that a larger amount of NH_3 interacts with Cu sites (i.e., Z2Cu and ZCuOH) compared to Brønsted acid sites. This well supports the higher Z2Cu population for Cu/SSZ-13 compared to Cu/ZSM-5 and Cu/BEA as discussed in relation to Figures 1 and 2.

The formation and subsequent decomposition of ammonium nitrate was thoroughly examined by performing ammonium nitrate temperature-programmed desorption (AN-TPD) experiments to gain fundamental understanding of the N_2O formation over the samples with different zeolite frameworks. Briefly, the experiment was composed of an exposure step with 200 ppm NH_3, 200 ppm NO_2, 10% O_2, and 5% H_2O at 150 or 200 °C for 1 h and thereafter purging followed by a heating ramp using 5% H_2O in Ar as inlet feed gas (see the Ammonium Nitrate Temperature-Programmed Desorption section for experimental details).

The experiments were conducted using monolith samples with the zeolites in the H and Cu forms, and the results are shown in Figures S6 and S7, respectively. The concentrations of NH_3, NO, NO_2, N_2, and N_2O (Figures S6 and S7) reach steady state during the 60 min exposure period for the H and Cu forms of ZSM-5 and BEA. However, this is not the case for the H/SSZ-13 and Cu/SSZ-13 samples, where AN formation still proceeds after 60 min exposure. N_2 is instantly produced when the samples simultaneously are exposed to NH_3 and NO_2. Potential pathways for N_2 formation are as follows: (1) SCR of NO_2 with NH_3 and (2) AN formation. It is well established that AN formation proceeds by NO_2 dimerization (R.1) and disproportionation (R.2)[54] to form surface nitrites and nitrates followed by the subsequent reaction of the nitrites and nitrates with NH_3 (R.3 and R.4), leading to N_2 and AN formation.[55,56] It should be mentioned that minor NO formation is observed when NH_3 + NO_2 is introduced as shown in Figures S6 and S7. This small instantaneous NO formation is due to the oxidation of surface nitrites by NO_2 forming surface nitrates via R.5.[10,57] The amount of NO formed is negligible compared to the produced AN. This indicates that surface nitrites are not oxidized by NO_2, but instead react with NH_3 forming N_2, suggesting that the prepared catalysts are highly active in NO_2 SCR with NH_3.

$$2NO_2 \leftrightarrow N_2O_4 \quad \text{(R.1)}$$

$$N_2O_4 + H_2O \leftrightarrow HONO + HNO_3 \quad \text{(R.2)}$$

$$NH_3 + HONO \leftrightarrow NH_4^+ + NO_2^- \leftrightarrow [NH_4NO_2] \rightarrow N_2 + 2H_2O \quad \text{(R.3)}$$

$$NH_3 + HNO_3 \leftrightarrow NH_4^+ + NO_3^- \leftrightarrow NH_4NO_3 \quad \text{(R.4)}$$

$$HNO_3 + NO \leftrightarrow HONO + NO_2 \quad \text{(R.5)}$$

For the H/SSZ-13 sample, only negligible N_2O formation is observed during the exposure step even at 200 °C, suggesting that AN is still residing inside the zeolite cages without thermal decomposition forming N_2O (SI, S2) even above the AN decomposition temperature. However, continuous N_2O formation is observed for the H/ZSM-5 and H/BEA samples at 200 °C but not at 150 °C for H/ZSM-5, showing lower stability for AN in H/ZSM-5 and H/BEA. Whereas, formation of N_2O is observed for all Cu/zeolite samples during the exposure period, but only minor amounts of N_2O are observed for the Cu/SSZ-13 sample at 150 °C, see Figure 4a. These results demonstrate that AN decomposition is enhanced in the presence of Cu species. In addition, it is clear that the N_2O formation during the exposure step increases in the order Cu/SSZ-13 < Cu/ZSM-5 < Cu/BEA.

The amount of AN was estimated by performing nitrogen mass balance calculations based on the detected NH_3, NO_2,

https://doi.org/10.1021/acs.iecr.1c02732
Ind. Eng. Chem. Res. 2021, 60, 17826−17839

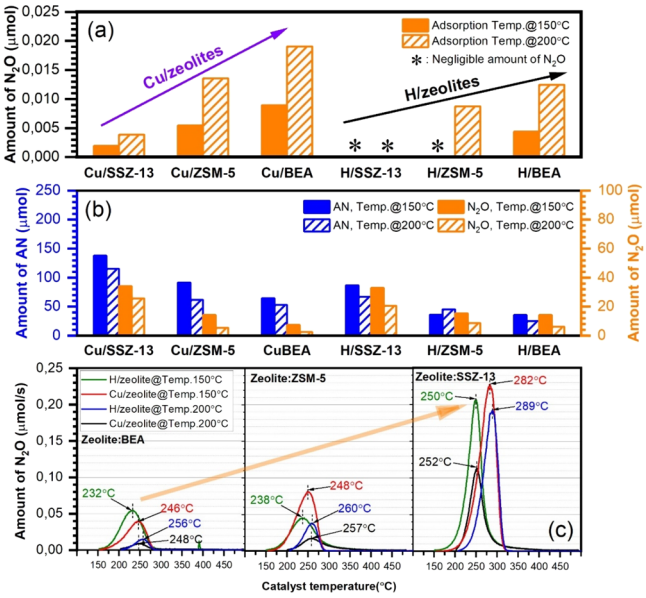

Figure 4. (a) Produced amount of N_2O during the exposure step in AN-TPD for the SSZ-13, ZSM-5, and BEA samples in the H and Cu forms. (b) Estimated amount of accumulated ammonium nitrate (AN) during the adsorption step and produced N_2O during the subsequent purging and desorption steps. (c) N_2O concentration as a function of sample temperature during purging and desorption period for the samples in H and Cu forms during AN-TPD (heating rate: 20 °C·min^{-1}).

N_2O, and N_2 during the purging and desorption steps in the AN-TPD experiment. A detailed description of the procedure can be found in the SI. The integrated amounts of the different gas species are reported in Figure S8. The results (Figure 4b) clearly show that the N_2O formation is connected to the produced amount of AN, indicating that N_2O originates from thermal decomposition of AN (SI, S2). Remarkably, the Cu and H forms of SSZ-13 show substantial AN and N_2O formation among the samples. Moreover, a higher AN formation for Cu/SSZ-13 below the AN decomposition temperature (maximum at 150 °C compared to 200 °C) is found. The reason could be that higher temperature does not favor the formation of N_2O_4;[58] thus, it results in a lower amount of surface nitrate groups than that at 150 °C. In addition, some of the AN will continuously decompose during the exposure step at higher temperature, reducing the amount of AN on the surface at 200 compared to 150 °C.

The N_2O formation during the desorption step of the AN-TPD experiment is depicted in Figure 4c. The formed N_2O originates from AN remaining inside the zeolite cages after the exposure step. Kwak et al.[24] observed that the N_2O formation during SCR conditions over Cu/zeolites follows the order Cu/SSZ-13 < Cu/ZSM-5 < Cu/BEA. We also observe the same trend during the continuous SCR reaction (Figure 6) and during the exposure step of the AN TPD (Figure 4a). This is due to the lower stability of AN in Cu/BEA (followed by Cu/ZSM-5), which facilitates the decomposition of AN to N_2O, as will be discussed below. Interestingly, co-exposure to NH_3 and NO_2 in the present study results in the opposite trend, namely, that a higher amount of N_2O is formed over SSZ-13 followed by ZSM-5 and BEA during the desorption step. Substantial N_2O formation is confirmed for both the H and Cu forms of SSZ-13 at 150 °C in Figure 4c. By comparing the temperature for N_2O formation maximum for the H and Cu forms, the stability of AN inside the zeolite cage is indicated. A high N_2O peak located at high temperature is seen for SSZ-13, showing high AN stability in this sample. Additionally, it is found that the Cu/zeolites show N_2O peaks at higher temperature than that of H/zeolites regardless of the pore size and channel system, meaning that AN is more strongly bound to the Cu sites compared to Brønsted acid sites. Thus, relatively higher energy is required to decompose AN species for Cu/zeolites.

In summary, AN formation and decomposition are strongly correlated with the zeolite framework, as well as Cu addition in NO_2 SCR. During the AN-TPD experiments, SSZ-13 exhibits the highest AN storage capacity and thereby also the highest N_2O formation during the desorption phase followed by ZSM-5 and BEA. NO_2 contains one unpaired electron and can combine with another NO_2 molecule to be stabilized in the gas phase. Its disproportionation is easily promoted into nitrate and nitrite ion pairs in zeolite pores having high polarity. In particular, a high concentration of framework Al and confined space in zeolite pores results in strong "solvent effects".[59] In this respect, SSZ-13 having a smaller cage size and higher 2-Al concentration based on the H_2-TPR experiments (Figure 1) and T−O−T vibration data (Figure 2) can result in a strong

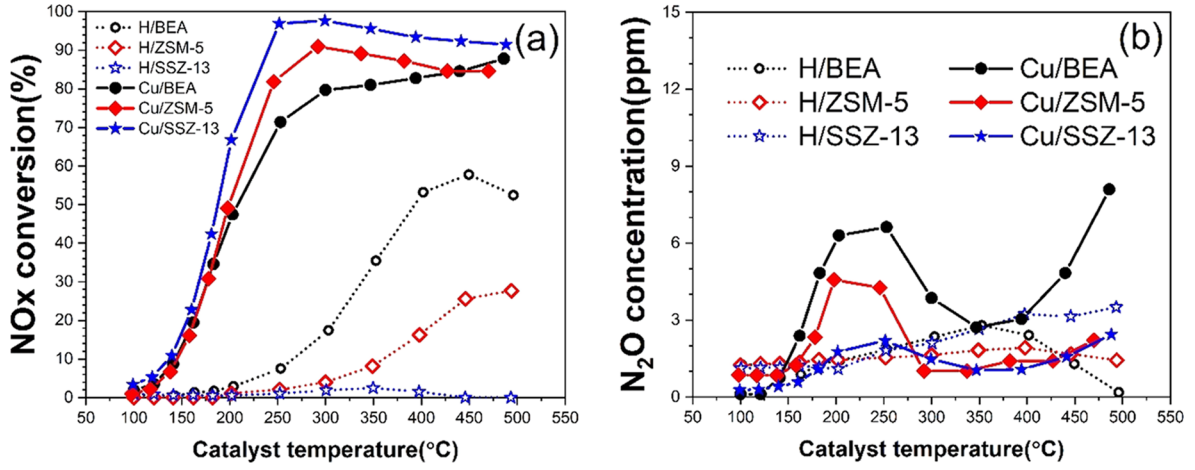

Figure 5. NOx conversion (a) and N_2O formation (b) as a function of catalyst temperature in standard SCR for the H and Cu forms of BEA, ZSM-5, and SSZ-13 (gas inlet: 400 ppm NH_3, 400 ppm NO, 10% O_2, 5% H_2O, GHSV = 20,400 h^{-1}, heating rate: 20 °C·min^{-1}).

https://doi.org/10.1021/acs.iecr.1c02732
Ind. Eng. Chem. Res. 2021, 60, 17826−17839

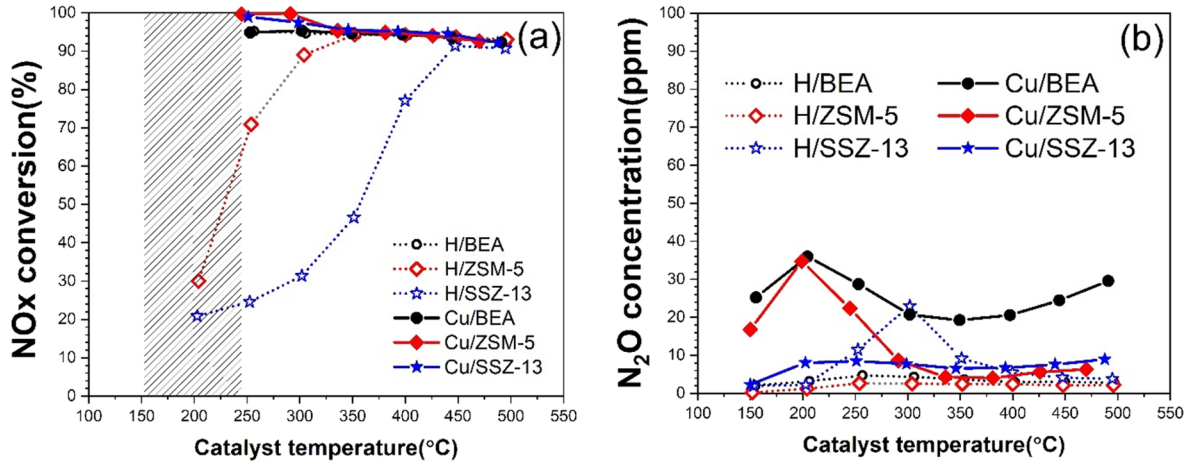

Figure 6. NOx conversion (a) and N_2O formation (b) as a function of catalyst temperature in fast SCR for the H and Cu forms of BEA, ZSM-5, and SSZ-13 (gas inlet: 400 ppm NH_3, 200 ppm NO, 200 ppm NO_2, 10% O_2, 5% H_2O, GHSV = 20,400 h^{-1}, heating rate: 20 °C min^{-1}).

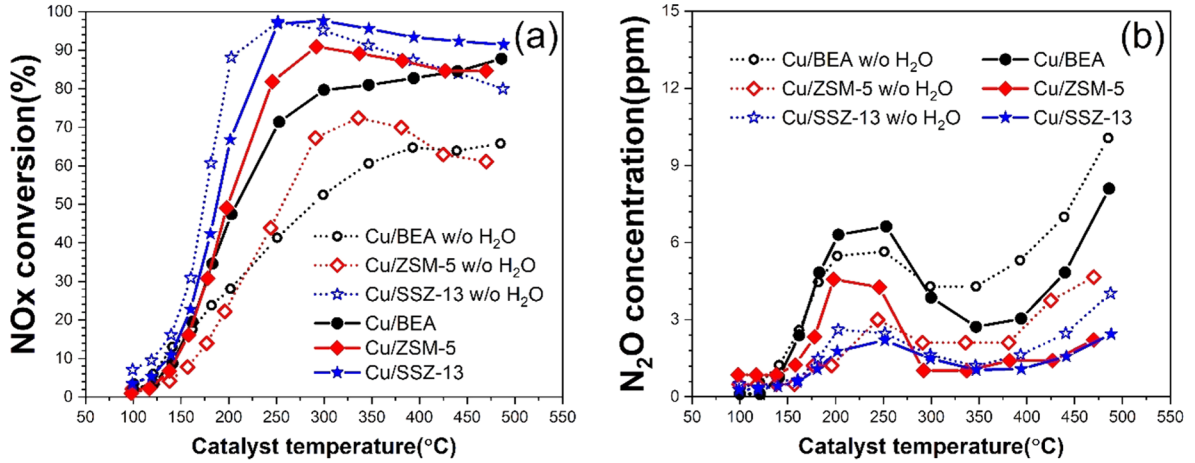

Figure 7. NOx conversion (a) and N_2O formation (b) as a function of catalyst temperature with effect of water in standard SCR for the Cu form of BEA, ZSM-5, and SSZ-13 (gas inlet: 400 ppm NH_3, 400 ppm NO, 10% O_2, GHSV = 20,400 h^{-1}, heating rate: 20 °C·min^{-1}).

polar environment. Therefore, SSZ-13 enhances the NO_2 disproportionation and produces more surface nitrate and nitrite species compared to ZSM-5 and BEA, leading to the highest AN formation over SSZ-13. Thus, we conclude that the zeolite framework (especially the Al coordination) has a significant effect on NO_2 disproportionation, which is promoted in the presence of Cu species. On the contrary, the trend is opposite for the continuous production of N_2O during the exposure step, where BEA produced the highest quantities. This is due to the low stability of AN in BEA, which results in a high continuous N_2O formation and thereby also a lower amount of AN remaining on the surface. Moreover, our results show that the addition of Cu enhances both the stability and formation of AN. Simultaneously, Cu also increases the continuous N_2O formation, and the reason for this could be the higher overall activity in the presence of Cu.

Catalytic Activity Measurements. *Effect of Copper Addition and Different Zeolite Framework.* In this section, the N_2O formation characteristics are assessed during activity tests for standard and fast SCR condition using monolith samples. It should be noted that the SCR reaction does not reach steady state at 150 and 200 °C for the fast SCR conditions and this is also the case for the Cu/SSZ-13 sample at 100 °C for standard SCR conditions (see Figure 6a).

Figure 5 shows the NOx conversion and N_2O formation as a function of catalyst temperature for standard SCR. A low amount of N_2O (less than 10 ppm) is observed for all samples. For the Cu/zeolite samples, two regions for N_2O formation are clearly observed. The extent of N_2O formation follows the order Cu/BEA > Cu/ZSM-5 > Cu/SSZ-13 in the temperature range of ca. 150−300 °C, which is in the same order as during the adsorption step of the AN-TPD experiment (see Figure 4a). Higher NOx conversion but lower N_2O formation is observed for Cu/SSZ-13 followed by Cu/ZSM-5 and Cu/BEA in the temperature range of 150−300 °C (see Figure 5b). Especially, the NOx conversion reaches almost 98% at 250 °C for Cu/SSZ-13. Interestingly, this typical bimodal N_2O profile is not observed in absence of Cu species for the H/zeolites, indicating that this bimodal trend is due to Cu species. Recently, Xi et al.[60] and Feng et al.[27] reported that N_2O formation is associated with side reactions over Cu-oxy species, suggesting that formation of nitrate species or NH_4NO_3 can be excluded as the main reaction pathway for N_2O formation at low temperature in standard SCR conditions.

Figure 6 shows the NOx conversion and N_2O concentration as a function of catalyst temperature in fast SCR for the samples in the H and Cu forms. For fast SCR, steady state is not reached at 150 °C, although the N_2O concentrations are

https://doi.org/10.1021/acs.iecr.1c02732
Ind. Eng. Chem. Res. 2021, 60, 17826−17839

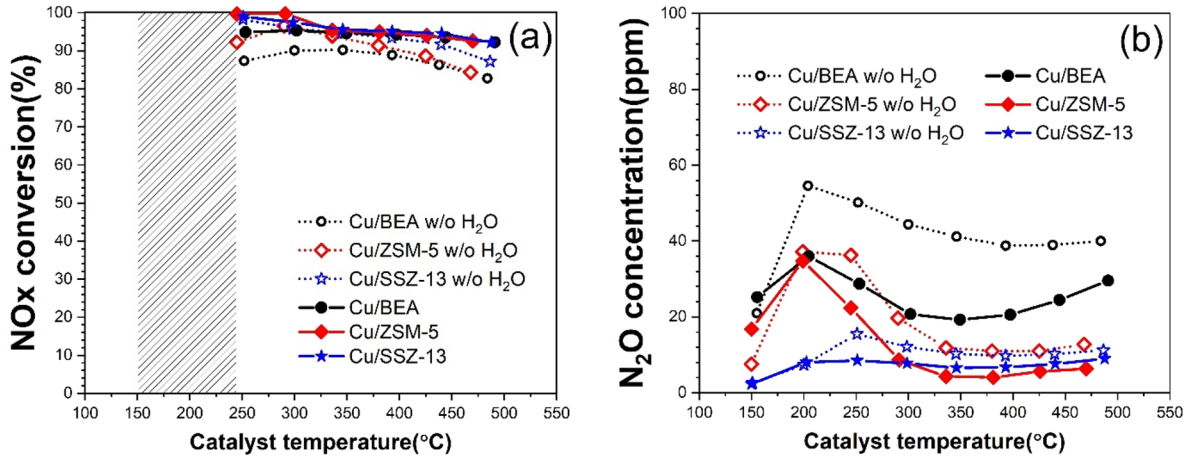

Figure 8. NOx conversion (a) and N_2O formation (b) as a function of catalyst temperature in fast SCR with effect of water for the H and Cu forms of BEA, ZSM-5, and SSZ-13 (gas inlet: 400 ppm NH_3, 200 ppm NO, 200 ppm NO_2, 10% O_2, 0 or 5% H_2O, GHSV = 20,400 h^{-1}, heating rate: 20 °C·min^{-1}).

approaching steady state (see Figure S10b). Especially, NO_2 is drastically consumed in comparison with NO. The H/zeolite samples and Cu/SSZ-13 clearly show inhibition of the SCR reaction at 150 °C during the 30 min under these conditions, while it is minor for the Cu/ZSM-5 and Cu/BEA (data not shown). It should be mentioned that the N_2O formation needs to be analyzed by taking time evolution into account (see Figure S10b) due to the high N_2O release when increasing the temperature between the steps. The results in Figure 6b show that the Cu/zeolite samples produce higher amounts of N_2O in comparison with the H/zeolites at 150 and 200 °C. Especially, higher formation of N_2O is observed for Cu/BEA followed by Cu/ZSM-5 and Cu/SSZ-13 at 150 and 200 °C, indicating continuous AN decomposition into N_2O. These results are in line with the findings discussed regarding the AN-TPD experiments.

Interestingly, when the temperature is increased, high N_2O formation is observed (50 ppm) from 200 to 250 °C for H/BEA and from 250 to 300 °C (260 ppm) for H/SSZ-13 (see Figure S10b). Especially, a strong N_2O peak is observed for H/SSZ-13, whereas insignificant N_2O formation is observed for the Cu/SSZ-13 sample. This observation suggests that AN in Cu/SSZ-13 is significantly reduced by NO through R.6 and that this AN reduction is enhanced in the presence of Cu species. Therefore, it results in low N_2O formation for Cu/SSZ-13 but a significant N_2O peak and formation in the absence of copper species for H/SSZ-13. Significantly higher amounts of N_2O are observed for the Cu/BEA and Cu/ZSM-5 samples compared to Cu/SSZ-13 at 200 °C (i.e., above AN decomposition temperature) due to the lower stability of AN in these zeolites, resulting in a continuous formation and decomposition of AN into N_2O.

$$NH_4NO_3 + NO \rightarrow NO_2 + NH_4NO_2 \quad \text{(R.6)}$$

Effect of Water Vapor. The effect of water vapor on N_2O formation was investigated under standard and fast SCR conditions for the Cu/zeolite samples (see Figures 7 and 8). It needs to be mentioned that the outlet NH_3 level during the standard SCR reaction at 100 °C does not reach steady state; thus, it is excluded in Figure S11a. This is also the case for fast SCR below 250 °C in NOx conversion (dashed region in Figure 8a).

Figure 7 shows the NOx conversion and N_2O formation as a function of catalyst temperature in the presence and absence of water vapor for the Cu/zeolite samples during standard SCR conditions. The water clearly influences the N_2O formation. It still shows two N_2O maxima in the low- and high-temperature regions. Interestingly, different effects are seen at ca. 100−300 and 300−500 °C. In the low-temperature region, less N_2O is formed over the Cu/BEA and Cu/ZSM-5 samples under dry conditions, while similar amounts of N_2O are formed under dry and wet conditions for Cu/SSZ-13. In the high-temperature region above 300 °C, more N_2O is formed under dry conditions. However, for all cases, the N_2O formation is quite low (less than 10 ppm N_2O).

Figure 8 shows the NOx conversion and N_2O formation in the presence and absence of water vapor for the different Cu/zeolite samples in fast SCR conditions. A significant effect of water is observed for the fast SCR conditions, where the N_2O formation increases in the absence of water over the entire experiment except at 150 °C. As mentioned above, the concentration of NO and NO_2 decreases gradually and does not reach steady state within the 30 min reaction time at 150 and 200 °C. For the Cu/SSZ-13 sample, a clear inhibition of the fast SCR reaction due to AN formation can be seen at low temperatures both in the presence and absence of water (see Figure S13).

AN-TPD experiments were carried out in the absence of water using the Cu/SSZ-13 sample, and the amount of AN was estimated through nitrogen mass balance calculations based on the purging and desorption steps. These results were compared with the AN-TPD in the presence of water. Figure S14 shows the concentrations of NH_3, NO, NO_2, N_2O, and N_2 from the dry AN-TPDs at 150 and 200 °C. Overall, the trends of the gas concentrations are similar to the case with water present (Figures S6 and S7), but the amounts differ. Figure 9a shows the effect of water vapor on N_2O formation during the desorption step in the AN-TPD over the Cu/SSZ-13 sample. A significant effect of water is seen, namely, higher amounts of N_2O are produced in the absence of water, which also is the case for the fast SCR conditions (Figure 9b). The N_2O formation starts at a lower temperature, and also the peak maximum is observed at a lower temperature in the absence of water in comparison to wet conditions. With respect to AN formation, more AN is produced in the absence of water (see

https://doi.org/10.1021/acs.iecr.1c02732
Ind. Eng. Chem. Res. 2021, 60, 17826−17839

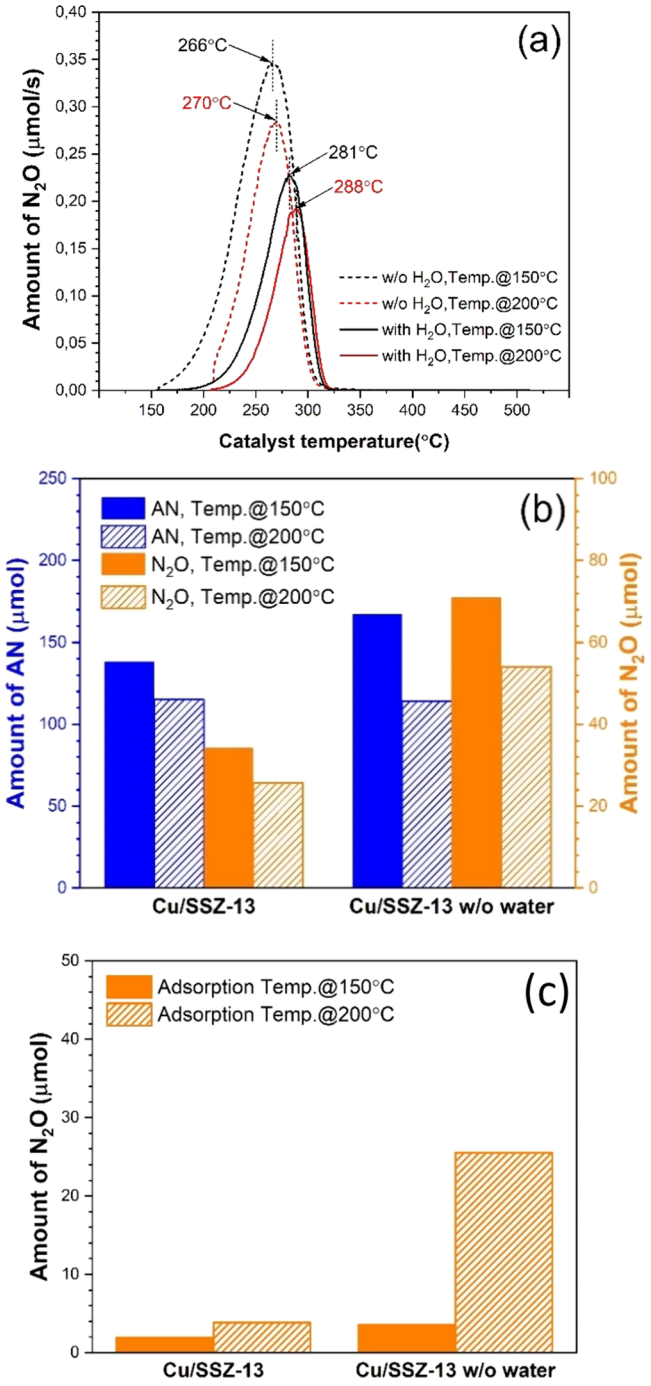

Figure 9. (a) Effect of water on N_2O formation over the Cu/SSZ-13 sample during AN-TPD. (b) Amount of ammonium nitrate and N_2O in AN-TPD in the presence or absence of water. (c) N_2O released during the adsorption step of the AN-TPD for Cu/SSZ-13 (gas inlet: 200 ppm NH_3, 200 ppm NO_2, 0 or 5% H_2O Ar bal, GHSV = 20,400 h^{-1}, heating rate: 20 °C·min^{-1}).

Figure 9b). Strong water inhibition of NO^+ and nitrate formation over Cu/CHA has been reported by Ruggeri et al.[54] They suggested that Cu dimers (i.e., $[Cu{-}O{-}Cu]^{2+}$) are the active sites for the efficient oxidation of NO to NO_2, and water dissociates the Cu dimers into $Cu^{2+}{-}OH$ groups. Therefore, breakage of the pairs of active Cu sites diminishes NO activation and leads to hindered nitrate formation, thereby resulting in lower AN formation in the presence of water vapor.

Interestingly, a similar amount of AN is formed in the presence and absence of water at 200 °C but the N_2O formation is higher under dry conditions in Figure 9b. These results indicate that the contribution of AN decomposition into NH_3 and HNO_3 increases in the presence of water. These results are supported by the fact that NO_2 and N_2 production increases at 200 °C in the presence of water (see Figure S15), suggesting that water promotes the selectivity for the AN decomposition into NH_3 and surface nitrate forming NO_2 (SI, S5). Note that a relatively higher amount of N_2O formation is observed during the exposure step in the absence of water at 200 °C in Figure 9c, suggesting that more AN is formed inside the zeolite pores under dry conditions, which is consistent with the results in Figure 9b.

The experimental results clearly show that water has a significant effect on the N_2O formation in standard and fast SCR conditions as well as on the AN-TPD results over Cu/zeolites. Interestingly, the different effect of water on the formation of N_2O at low temperatures for Cu/SSZ-13 in standard SCR can be due to that the configuration of active Cu species is different in Cu/SSZ-13 compared to Cu/ZSM-5 and Cu/BEA. In contrast, totally different effects of water are observed for Cu/zeolites in fast SCR conditions at low temperature with clear deactivation at 150 °C (see Figure S13) due to AN formation, especially under dry conditions. At 200 °C, significantly improved NOx conversion is observed, which is due to decomposition of formed AN by water via the SI, S5, for Cu/SSZ-13. This indicates that the catalytic active sites are less blocked by AN; thus, it is possible to achieve higher SCR activity. Indeed, the NOx conversion significantly increases with decreased N_2O formation in the presence of water due to more available catalytic active sites for fast SCR (see Figure S13) at 200 °C. The results suggest that there are at least two different reaction pathways for low-temperature N_2O formation in fast SCR, resulting from the side reaction via Cu-oxy species and AN decomposition to N_2O.

N_2O formation over H and Cu/Zeolites. The low-temperature N_2O formation mechanism is lively discussed. As mentioned above, Xi et al.[60] and Feng et al.[27] have suggested that Cu-oxy species is the active site for the low-temperature N_2O formation in standard SCR. Specifically, their suggested Cu configuration is NH_3 solvated Cu-peroxo complexes (i.e., $[Cu_2(NH_3)_4O_2]^{2+}$). Also, Cu ion pairs are observed for Cu/BEA and Cu/ZSM-5, but the difference is that it is oxygen-bridged copper dimers (i.e., $[Cu{-}O{-}Cu]^{2+}$).[52,61,62] Villamaina et al.[63] performed CO oxidation at low temperature over Cu/CHA to probe Cu−oxo dimers as active Cu^{2+} species, and the results show second order dependence of the rate of CO_2 formation with reduction of two $[Cu^{2+}{-}OH]^+$ sites. In this respect, our H_2-TPR results in Figure 1b show that Cu/BEA (52% $[Cu^{2+}{-}OH]^+$ of the total Cu content) can have a higher amount of binuclear Cu-oxo species followed by Cu/ZSM-5 and Cu/SSZ-13. This can explain the observed N_2O formation trend Cu/BEA > Cu/ZSM-5 > Cu/SSZ-13 in standard SCR in the low-temperature region without inhibition of the NOx reduction. Note that it is possible to have different Cu-peroxo complex configurations with respect to different zeolite frameworks; indeed different physical and chemical environments are confirmed by the observed larger distortion of Cu species for Cu/SSZ-13 in Table 1, plausibly leading to the different N_2O formation trends. Further investigations are however needed to define the configuration of the active Cu sites and how different Cu-oxy

https://doi.org/10.1021/acs.iecr.1c02732
Ind. Eng. Chem. Res. 2021, 60, 17826−17839

species affect the N_2O formation over different zeolite frameworks.

On the contrary, inhibition of the SCR reaction is clearly observed in fast SCR, especially in the case of Cu/SSZ-13 (see Figure S13 at 150 °C). Significant deactivation and high consumption of NO_2 indicate the formation of NH_4NO_3. Moreover, the considerable N_2O formation for H/SSZ-13 suggests that another N_2O formation pathway exits in contrast to N_2O formation over Cu−dimer complexes in standard SCR. Significantly lower NOx conversion is generally observed when the NO_2 fraction exceeds 50% of the total NOx at low temperature (below 200 °C).[60] This indicates that surface nitrate or nitrate species formation is dominant, leading to higher AN formation at low temperature. Furthermore, different thermal stability of AN is observed in the presence or absence of Cu species in the AN-TPD experiments (see Figure 4c). The AN thermal stability trend over different zeolite frameworks (SSZ-13 > ZSM-5 > BEA) is reported by several research groups, and a pore-confinement effect has been suggested to explain the remarkably strong thermal stability of AN over the CHA framework.[21,23,24] For the fast SCR reaction, we observe continuous N_2O formation in the descending order Cu/BEA > Cu/ZSM-5 > Cu/SSZ-13. The reason that Cu/BEA forms the highest amount of N_2O is likely due to the low stability of AN. However, we observed the same N_2O formation trend during standard SCR conditions (Cu/BEA > Cu/ZSM-5 > Cu/SSZ-13), where AN formation is not likely. Thus, the pore-confinement cannot be used to explain the N_2O results during standard SCR. Using DFT calculations, Feng et al.[27] suggested that Brønsted acid sites can catalyze AN decomposition and AN stability can hence be affected by the acidity of the CHA framework. Interestingly, the observed Brønsted acidity in Figure 3 for the CHA, MFI, and BEA frameworks is in line with the AN formation trend in Figure 4c. Therefore, we hypothesize that the N_2O formation trend resulting from AN might be due to the different Brønsted acidity of the zeolites resulting from the different lattice arrangements of the Al atoms in the zeolite framework.

CONCLUSIONS

N_2O formation was investigated in terms of Cu species, zeolite framework, and water vapor over different zeolite frameworks (i.e., CHA, MFI, BEA) functionalized by Cu. The intrinsic features of the CHA, MFI, and BEA frameworks affect the speciation of Cu ions and the catalytic DeNOx performance and N_2O formation. H_2-TPR and DRIFTS show that the CHA framework has an abundance of 2Al sites, promoting NO_2 disproportionation due to the stronger polar environment inside the CHA cage compared to the MFI and BEA frameworks. Therefore, the actual AN and N_2O formation trend follows the order Cu/SSZ-13 > Cu/ZSM-5 > Cu/BEA. However, the opposite trend is observed under fast SCR conditions because of the different stability of AN leading to the N_2O formation, which follows the trend Cu/BEA > Cu/ZSM-5 > Cu/SSZ-13.

Water was found to have a significant effect on both AN formation and decomposition. Water inhibits AN formation due to the cleavage of the Cu-dimer complexes into Cu−OH groups, resulting in lower NO oxidation and surface nitrate formation. Furthermore, water promotes the N_2 selectivity via AN decomposition into NH_3 and HNO_3 forming more NO_2 compared to N_2O. Thus, we observed less N_2O formation under fast SCR in wet conditions.

The strong thermal stability of AN in the CHA framework and its impact on the N_2O formation mechanism remain a question. We suggest that the N_2O formation trend, which results from AN stability, is due to the different zeolite acidities and their different acidities result from the different lattice arrangements of Al atoms.

ASSOCIATED CONTENT

Supporting Information

The Supporting Information is available free of charge at https://pubs.acs.org/doi/10.1021/acs.iecr.1c02732.

More details on the zeolite synthesis, characterization results, and experimental methods in terms of ammonium nitrate temperature-programmed desorption (protocols, blank experiment, SO_2 effect, concentration traces of NO, NO_2, N_2, NH_3, N_2O); integrals of NH_3, N_2, NO_2 during purging and desorption steps; and NH_3 conversion with concentration trace of N_2O in standard and fast SCR conditions (PDF)

AUTHOR INFORMATION

Corresponding Author

Louise Olsson − *Department of Chemistry and Chemical Engineering, Competence Centre for Catalysis, Chalmers University of Technology, Gothenburg 41296, Sweden;* orcid.org/0000-0002-8308-0784; Phone: +46 (0)31 7724390; Email: louise.olsson@chalmers.se

Authors

Joonsoo Han − *Department of Chemistry and Chemical Engineering, Competence Centre for Catalysis, Chalmers University of Technology, Gothenburg 41296, Sweden*

Aiyong Wang − *Department of Chemistry and Chemical Engineering, Competence Centre for Catalysis, Chalmers University of Technology, Gothenburg 41296, Sweden*

Ghodsieh Isapour − *Department of Chemistry and Chemical Engineering, Competence Centre for Catalysis, Chalmers University of Technology, Gothenburg 41296, Sweden*

Hanna Härelind − *Department of Chemistry and Chemical Engineering, Competence Centre for Catalysis, Chalmers University of Technology, Gothenburg 41296, Sweden;* orcid.org/0000-0002-9564-4276

Magnus Skoglundh − *Department of Chemistry and Chemical Engineering, Competence Centre for Catalysis, Chalmers University of Technology, Gothenburg 41296, Sweden;* orcid.org/0000-0001-7946-7137

Derek Creaser − *Department of Chemistry and Chemical Engineering, Competence Centre for Catalysis, Chalmers University of Technology, Gothenburg 41296, Sweden*

Complete contact information is available at: https://pubs.acs.org/10.1021/acs.iecr.1c02732

Author Contributions

The manuscript was written through contributions of all authors. All authors have given approval to the final version of the manuscript.

Notes

The authors declare no competing financial interest.

ACKNOWLEDGMENTS

This work has been performed within the Competence Centre for Catalysis, which is hosted by Chalmers University of

Technology and financially supported by the Swedish Energy Agency, Chalmers, and the member companies AB Volvo, ECAPS AB, Johnson Matthey AB, Preem AB, Scania CV AB, and Umicore Denmark ApS. We would like to acknowledge the International Zeolite Association (IZA) for providing electronic sources of the framework structure for the graphical abstract.

REFERENCES

(1) Ottinger, N.; Schmidt, N.; Liu, Z. G., *Understanding System- and Component-Level N2O Emissions from a Vanadium-Based Nonroad Diesel Aftertreatment System*. SAE International: 2017.
(2) Han, J.; Kim, T.; Jung, H.; Pyo, S.; Cho, G.; Oh, Y.; Kim, H. Improvement of NOX Reduction Rate of Urea SCR System Applied for an Non-Road Diesel Engine. *Int. J. Automot. Technol.* **2019**, *20*, 1153−1160.
(3) Kamasamudram, K.; Henry, C.; Currier, N.; Yezerets, A. N2O Formation and Mitigation in Diesel Aftertreatment Systems. *SAE Int. J. Engines* **2012**, *5*, 688−698.
(4) Jansson, J.; Johansson, Å.; Sjovall, H.; Larsson, M.; Smedler, G.; Newman, C.; Pless, J., *Heavy Duty Emission Control System Analysis and Optimization for Future Demands*. SAE International: 2015.
(5) Kamasamudram, K.; Currier, N. W.; Chen, X.; Yezerets, A. Overview of the practically important behaviors of zeolite-based urea-SCR catalysts, using compact experimental protocol. *Catal. Today* **2010**, *151*, 212−222.
(6) Sandro, B.; Oliver, K.; Arno, T.; Roderik, A. The State of the Art in Selective Catalytic Reduction of NOx by Ammonia Using Metal-Exchanged Zeolite Catalysts. *Catal. Rev.* **2008**, *50*, 492−531.
(7) Zhang, D.; Yang, R. T. N2O Formation Pathways over Zeolite-Supported Cu and Fe Catalysts in NH3-SCR. *Energy Fuels* **2018**, *32*, 2170−2182.
(8) Liu, B.; Yao, D.; Wu, F.; Wei, L.; Li, X.; Wang, X. Experimental Investigation on N2O Formation during the Selective Catalytic Reduction of NOx with NH3 over Cu-SSZ-13. *Ind. Eng. Chem. Res.* **2019**, *58*, 20516−20527.
(9) Shan, Y.; Shi, X.; He, G.; Liu, K.; Yan, Z.; Yu, Y.; He, H. Effects of NO2 Addition on the NH3-SCR over Small-Pore Cu−SSZ-13 Zeolites with Varying Cu Loadings. *J. Phys. Chem. C* **2018**, *122*, 25948−25953.
(10) Luo, J.; Tang, Y.; Joshi, S.; Kamasamudram, K.; Currier, N.; Yezerets, A. The Impact of Ammonium Nitrate Species on Low Temperature NOx Conversion Over Cu/CHA SCR Catalyst. *SAE Int. J. Engines* **2017**, *10*, 1691−1696.
(11) Olsson, L.; Wijayanti, K.; Leistner, K.; Kumar, A.; Joshi, S. Y.; Kamasamudram, K.; Currier, N. W.; Yezerets, A. A multi-site kinetic model for NH3-SCR over Cu/SSZ-13. *Appl. Catal., B* **2015**, *174-175*, 212−224.
(12) Paolucci, C.; Di Iorio, J. R.; Schneider, W. F.; Gounder, R. Solvation and Mobilization of Copper Active Sites in Zeolites by Ammonia: Consequences for the Catalytic Reduction of Nitrogen Oxides. *Acc. Chem. Res.* **2020**, *53*, 1881−1892.
(13) Oda, A.; Shionoya, H.; Hotta, Y.; Takewaki, T.; Sawabe, K.; Satsuma, A. Spectroscopic Evidence of Efficient Generation of Dicopper Intermediate in Selective Catalytic Reduction of NO over Cu-Ion-Exchanged Zeolites. *ACS Catal.* **2020**, *10*, 12333−12339.
(14) Negri, C.; Selleri, T.; Borfecchia, E.; Martini, A.; Lomachenko, K. A.; Janssens, T. V. W.; Cutini, M.; Bordiga, S.; Berlier, G. Structure and Reactivity of Oxygen-Bridged Diamino Dicopper(II) Complexes in Cu-Ion-Exchanged Chabazite Catalyst for NH3-Mediated Selective Catalytic Reduction. *J. Am. Chem. Soc.* **2020**, *142*, 15884−15896.
(15) Liu, C.; Kubota, H.; Amada, T.; Kon, K.; Toyao, T.; Maeno, Z.; Ueda, K.; Ohyama, J.; Satsuma, A.; Tanigawa, T.; Tsunoji, N.; Sano, T.; Shimizu, K.-i. In Situ Spectroscopic Studies on the Redox Cycle of NH3−SCR over Cu−CHA Zeolites. *ChemCatChem* **2020**, *12*, 3050−3059.
(16) Gao, F.; Mei, D.; Wang, Y.; Szanyi, J.; Peden, C. H. Selective Catalytic Reduction over Cu/SSZ-13: Linking Homo- and Heterogeneous Catalysis. *J. Am. Chem. Soc.* **2017**, *139*, 4935−4942.
(17) Colombo, M.; Nova, I.; Tronconi, E. A comparative study of the NH3-SCR reactions over a Cu-zeolite and a Fe-zeolite catalyst. *Catal. Today* **2010**, *151*, 223−230.
(18) Yuan, X.; Liu, H.; Gao, Y. Diesel Engine SCR Control: Current Development and Future Challenges. *Emiss. Control Sci. Technol.* **2015**, *1*, 121−133.
(19) Wang, D.; Zhang, L.; Kamasamudram, K.; Epling, W. S. In Situ-DRIFTS Study of Selective Catalytic Reduction of NOx by NH3 over Cu-Exchanged SAPO-34. *ACS Catal.* **2013**, *3*, 871−881.
(20) Gao, F.; Kwak, J. H.; Szanyi, J.; Peden, C. H. F. Current Understanding of Cu-Exchanged Chabazite Molecular Sieves for Use as Commercial Diesel Engine DeNOx Catalysts. *Top. Catal.* **2013**, *56*, 1441−1459.
(21) Chen, H.-Y.; Wei, Z.; Kollar, M.; Gao, F.; Wang, Y.; Szanyi, J.; Peden, C. H. F. A comparative study of N2O formation during the selective catalytic reduction of NOx with NH3 on zeolite supported Cu catalysts. *J. Catal.* **2015**, *329*, 490−498.
(22) Kubota, H.; Liu, C.; Toyao, T.; Maeno, Z.; Ogura, M.; Nakazawa, N.; Inagaki, S.; Kubota, Y.; Shimizu, K.-i. Formation and Reactions of NH4NO3 during Transient and Steady-State NH3-SCR of NOx over H-AFX Zeolites: Spectroscopic and Theoretical Studies. *ACS Catal.* **2020**, *10*, 2334−2344.
(23) Kwak, J. H.; Tonkyn, R. G.; Kim, D. H.; Szanyi, J.; Peden, C. H. F. Excellent activity and selectivity of Cu-SSZ-13 in the selective catalytic reduction of NOx with NH3. *J. Catal.* **2010**, *275*, 187−190.
(24) Kwak, J. H.; Tran, D.; Burton, S. D.; Szanyi, J.; Lee, J. H.; Peden, C. H. F. Effects of hydrothermal aging on NH3-SCR reaction over Cu/zeolites. *J. Catal.* **2012**, *287*, 203−209.
(25) Chen, H.-Y., Cu/Zeolite SCR Catalysts for Automotive Diesel NOx Emission Control. In *Urea-SCR Technology for deNOx After Treatment of Diesel Exhausts*, Nova, I.; Tronconi, E., Eds. Springer New York: New York, NY, 2014; pp. 123−147.
(26) Mihai, O.; Widyastuti, C. R.; Andonova, S.; Kamasamudram, K.; Li, J. H.; Joshi, S. Y.; Currier, N. W.; Yezerets, A.; Olsson, L. The effect of Cu-loading on different reactions involved in NH3-SCR over Cu-BEA catalysts. *J. Catal.* **2014**, *311*, 170−181.
(27) Feng, Y.; Janssens, T. V. W.; Vennestrøm, P. N. R.; Jansson, J.; Skoglundh, M.; Grönbeck, H. The Role of H+- and Cu+-Sites for N2O Formation during NH3-SCR over Cu-CHA. *J. Phys. Chem. C* **2021**, *125*, 4595−4601.
(28) Gao, F.; Washton, N. M.; Wang, Y.; Kollár, M.; Szanyi, J.; Peden, C. H. F. Effects of Si/Al ratio on Cu/SSZ-13 NH3-SCR catalysts: Implications for the active Cu species and the roles of Brønsted acidity. *J. Catal.* **2015**, *331*, 25−38.
(29) Wang, A.; Arora, P.; Bernin, D.; Kumar, A.; Kamasamudram, K.; Olsson, L. Investigation of the robust hydrothermal stability of Cu/LTA for NH3-SCR reaction. *Appl. Catal., B* **2019**, *246*, 242−253.
(30) Chaturvedi, S.; Dave, P. N. Review on Thermal Decomposition of Ammonium Nitrate. *J. Energ. Mater.* **2013**, *31*, 1−26.
(31) Shwan, S.; Skoglundh, M.; Lundegaard, L. F.; Tiruvalam, R. R.; Janssens, T. V. W.; Carlsson, A.; Vennestrøm, P. N. R. Solid-State Ion-Exchange of Copper into Zeolites Facilitated by Ammonia at Low Temperature. *ACS Catal.* **2015**, *5*, 16−19.
(32) Auvray, X.; Arvanitidou, M.; Högström, Å.; Jansson, J.; Fouladvand, S.; Olsson, L. Comparative Study of SO2 and SO2/SO3 Poisoning and Regeneration of Cu/BEA and Cu/SSZ-13 for NH3 SCR. *Emiss. Control Sci. Technol.* **2021**, 232.
(33) Ryu, T.; Kim, H.; Hong, S. B. Nature of active sites in Cu-LTA NH3-SCR catalysts: A comparative study with Cu-SSZ-13. *Appl. Catal., B* **2019**, *245*, 513−521.
(34) Wang, H.; Xu, R.; Jin, Y.; Zhang, R. Zeolite structure effects on Cu active center, SCR performance and stability of Cu-zeolite catalysts. *Catal. Today* **2019**, *327*, 295−307.
(35) Kwak, J. H.; Zhu, H.; Lee, J. H.; Peden, C. H.; Szanyi, J. Two different cationic positions in Cu-SSZ-13? *Chem. Commun.* **2012**, *48*, 4758−4760.

https://doi.org/10.1021/acs.iecr.1c02732
Ind. Eng. Chem. Res. 2021, 60, 17826−17839

(36) Beale, A. M.; Gao, F.; Lezcano-Gonzalez, I.; Peden, C. H. F.; Szanyi, J. Recent advances in automotive catalysis for NOx emission control by small-pore microporous materials. *Chem. Soc. Rev.* **2015**, *44*, 7371−7405.
(37) Giordanino, F.; Borfecchia, E.; Lomachenko, K. A.; Lazzarini, A.; Agostini, G.; Gallo, E.; Soldatov, A. V.; Beato, P.; Bordiga, S.; Lamberti, C. Interaction of NH3 with Cu-SSZ-13 Catalyst: A Complementary FTIR, XANES, and XES Study. *J. Phys. Chem. Lett.* **2014**, *5*, 1552−1559.
(38) Wang, A.; Olsson, L. Insight into the SO2 poisoning mechanism for NOx removal by NH3-SCR over Cu/LTA and Cu/SSZ-13. *Chem. Eng. J.* **2020**, *395*, 125048.
(39) Tkachenko, O. P.; Klementiev, K. V.; van den Berg, M. W. E.; Koc, N.; Bandyopadhyay, M.; Birkner, A.; Wöll, C.; Gies, H.; Grünert, W. Reduction of Copper in Porous Matrixes. Stepwise and Autocatalytic Reduction Routes. *J. Phys. Chem. B* **2005**, *109*, 20979−20988.
(40) Nanba, T.; Masukawa, S.; Ogata, A.; Uchisawa, J.; Obuchi, A. Active sites of Cu-ZSM-5 for the decomposition of acrylonitrile. *Appl. Catal., B* **2005**, *61*, 288−296.
(41) Gao, F.; Walter, E. D.; Karp, E. M.; Luo, J.; Tonkyn, R. G.; Kwak, J. H.; Szanyi, J.; Peden, C. H. F. Structure−activity relationships in NH3-SCR over Cu-SSZ-13 as probed by reaction kinetics and EPR studies. *J. Catal.* **2013**, *300*, 20−29.
(42) Martins, L.; Pablo, R.; Peguin, S.; Urquieta-Gonzalez, E. A. Cu and Co exchanged ZSM-5 zeolites: activity towards no reduction and hydrocarbon oxidation. *Quim. Nova.* **2006**, 223.
(43) Kefirov, R.; Penkova, A.; Hadjiivanov, K.; Dzwigaj, S.; Che, M. Stabilization of Cu+ ions in BEA zeolite: Study by FTIR spectroscopy of adsorbed CO and TPR. *Microporous Mesoporous Mater.* **2008**, *116*, 180−187.
(44) Cheng, X.; Su, D.; Wang, Z.; Ma, C.; Wang, M. Catalytic reduction of nitrogen oxide by carbon monoxide, methane and hydrogen over transition metals supported on BEA zeolites. *Int. J. Hydrogen Energy* **2018**, *43*, 21969−21981.
(45) Hajjar, R.; Millot, Y.; Man, P. P.; Che, M.; Dzwigaj, S. Two Kinds of Framework Al Sites Studied in BEA Zeolite by X-ray Diffraction, Fourier Transform Infrared Spectroscopy, NMR Techniques, and V Probe. *J. Phys. Chem. C* **2008**, *112*, 20167−20175.
(46) Pereda-Ayo, B.; De La Torre, U.; Illán-Gómez, M. J.; Bueno-López, A.; González-Velasco, J. R. Role of the different copper species on the activity of Cu/zeolite catalysts for SCR of NOx with NH3. *Appl. Catal., B* **2014**, *147*, 420−428.
(47) Paolucci, C.; Parekh, A. A.; Khurana, I.; Di Iorio, J. R.; Li, H.; Albarracin Caballero, J. D.; Shih, A. J.; Anggara, T.; Delgass, W. N.; Miller, J. T.; Ribeiro, F. H.; Gounder, R.; Schneider, W. F. Catalysis in a Cage: Condition-Dependent Speciation and Dynamics of Exchanged Cu Cations in SSZ-13 Zeolites. *J. Am. Chem. Soc.* **2016**, *138*, 6028−6048.
(48) Deka, U.; Lezcano-Gonzalez, I.; Weckhuysen, B. M.; Beale, A. M. Local Environment and Nature of Cu Active Sites in Zeolite-Based Catalysts for the Selective Catalytic Reduction of NOx. *ACS Catal.* **2013**, *3*, 413−427.
(49) Sobalík, Z.; Tvarůžková, Z.; Wichterlová, B. Skeletal T−O−T Vibrations as a Tool for Characterization of Divalent Cation Complexation in Ferrierite. *J. Phys. Chem. B* **1998**, *102*, 1077−1085.
(50) Sobalik, Z.; Šponer, J. E.; Wichterlová, B. Experimental and theoretical description of transition metal ion structures in zeolites relevant to deNOx catalysis. *Stud. Surf. Sci. Catal.* **2000**, *130*, 1463−1468.
(51) Broclawik, E.; Datka, J.; Gil, B.; Kozyra, P. T−O−T skeletal vibration in CuZSM-5 zeolite: IR study and quantum chemical modeling. *Phys. Chem. Chem. Phys.* **2000**, *2*, 401−405.
(52) Giordanino, F.; Vennestrøm, P. N.; Lundegaard, L. F.; Stappen, F. N.; Mossin, S.; Beato, P.; Bordiga, S.; Lamberti, C. Characterization of Cu-exchanged SSZ-13: a comparative FTIR, UV-Vis, and EPR study with Cu-ZSM-5 and Cu-beta with similar Si/Al and Cu/Al ratios. *Dalton Trans.* **2013**, *42*, 12741−12761.
(53) Deka, U.; Juhin, A.; Eilertsen, E. A.; Emerich, H.; Green, M. A.; Korhonen, S. T.; Weckhuysen, B. M.; Beale, A. M. Confirmation of Isolated Cu2+ Ions in SSZ-13 Zeolite as Active Sites in NH3-Selective Catalytic Reduction. *J. Phys. Chem. C* **2012**, *116*, 4809−4818.
(54) Ruggeri, M. P.; Nova, I.; Tronconi, E.; Pihl, J. A.; Toops, T. J.; Partridge, W. P. In-situ DRIFTS measurements for the mechanistic study of NO oxidation over a commercial Cu-CHA catalyst. *Appl. Catal., B* **2015**, *166-167*, 181−192.
(55) Grossale, A.; Nova, I.; Tronconi, E.; Chatterjee, D.; Weibel, M. The chemistry of the NO/NO2−NH3 "fast" SCR reaction over Fe-ZSM5 investigated by transient reaction analysis. *J. Catal.* **2008**, *256*, 312−322.
(56) Colombo, M.; Nova, I.; Tronconi, E. Detailed kinetic modeling of the NH3−NO/NO2 SCR reactions over a commercial Cu-zeolite catalyst for Diesel exhausts after treatment. *Catal. Today* **2012**, *197*, 243−255.
(57) Colombo, M.; Nova, I.; Tronconi, E. NO2 adsorption on Fe- and Cu-zeolite catalysts: The effect of the catalyst red−ox state. *Appl. Catal., B* **2012**, *111-112*, 433−444.
(58) Yeom, Y. H.; Henao, J.; Li, M. J.; Sachtler, W. M. H.; Weitz, E. The role of NO in the mechanism of NOx reduction with ammonia over a BaNa−Y catalyst. *J. Catal.* **2005**, *231*, 181−193.
(59) Pidko, E. A.; Mignon, P.; Geerlings, P.; Schoonheydt, R. A.; van Santen, R. A. A Periodic DFT Study of N2O4 Disproportionation on Alkali-Exchanged Zeolites X. *J. Phys. Chem. C* **2008**, *112*, 5510−5519.
(60) Xi, Y.; Ottinger, N. A.; Keturakis, C. J.; Liu, Z. G. Dynamics of low temperature N2O formation under SCR reaction conditions over a Cu-SSZ-13 catalyst. *Appl. Catal., B* **2021**, *294*, 120245.
(61) Da Costa, P.; Modén, B.; Meitzner, G. D.; Lee, D. K.; Iglesia, E. Spectroscopic and chemical characterization of active and inactive Cu species in NO decomposition catalysts based on Cu-ZSM5. *Phys. Chem. Chem. Phys.* **2002**, *4*, 4590−4601.
(62) Woertink, J. S.; Smeets, P. J.; Groothaert, M. H.; Vance, M. A.; Sels, B. F.; Schoonheydt, R. A.; Solomon, E. I. A [Cu2O]2+ core in Cu-ZSM-5, the active site in the oxidation of methane to methanol. *Proc. Natl. Acad. Sci.* **2009**, *106*, 18908−18913.
(63) Villamaina, R.; Iacobone, U.; Nova, I.; Ruggeri, M. P.; Collier, J.; Thompsett, D.; Tronconi, E. Low-T CO Oxidation over Cu−CHA Catalysts in Presence of NH3: Probing the Mobility of CuII Ions and the Role of Multinuclear CuII Species. *ChemCatChem* **2020**, *12*, 3843−3848.

https://doi.org/10.1021/acs.iecr.1c02732
Ind. Eng. Chem. Res. 2021, 60, 17826−17839